To appear in the *Journal of Hydraulic Research*
Vol. 00, No. 00, Month 20XX, 1–24

Research paper

Mechanisms that lead to violent geysers in vertical shafts

ARTURO S. LEON (IAHR Member), Associate Professor, *Department of Civil and Environmental Engineering, University of Houston, Houston, Texas, United States*
Email: aleon3@uh.edu (author for correspondence)

v1.0 released June 2016

Mechanisms that lead to violent geysers in vertical shafts

ABSTRACT

Supported with laboratory observations, this paper describes the mechanisms that lead to violent eruptions in stormwater and combined sewer systems. This paper also derives the upper limit for the geyser eruption velocity in these systems. The mathematical analysis shows that the maximum velocity of a gas-liquid mixture eruption in a vertical shaft is that of its mixture sound speed. The analysis also shows that the pressure gradient $\partial p/\partial z$ needs to increase substantially for the eruption velocity to approach the air-water mixture sound speed. The derived upper limit for the geyser eruption velocity is assessed using two test cases: A geyser event in a stormwater collection system in Minneapolis and our laboratory experiments.

Keywords: Combined sewer overflows; combined sewer system; geyser; stormwater; transient; violent eruption

1 Introduction

In general, stormwater (SW) and combined sewer systems (CSSs) consist of near-horizontal tunnels and vertical shafts, the latter of which serve as ventilation columns, access points for maintenance and/or as flow entry points to these systems. A geyser in these systems is a high frequency oscillatory release of a mixture of gas and liquid that occurs at vertical shafts. The oscillating jet of gas-liquid mixture may reach a height of the order of a few to tens of meters above ground level. Most geyser videos available in the web show multiple independent geyser events (e.g., `http://www.youtube.com/watch?v=4aQySL0sKys`), each of which consisted of several eruptions. Each independent geyser is very likely associated to a different isolated air pocket. Wright, Lewis, and Vasconcelos (2011) in their study of geyser events in a stormwater collection system in Minneapolis, identified nine independent geysers, each of which consisted of several eruptions, and each geyser lasted for about 10-25 s with about 75-90 s separating the onset of each geyser. Violent geysers are highly destructive. Many combined sewer systems are operated at a fraction of their maximum capacity to avoid transients and geysers (e.g., Leon, Ghidaoui, Schmidt, and García 2006; Leon, 2006). Operating CSSs at a fraction of their full capacity means that these systems are not fully utilized and hence, combined sewer overflows (CSOs) occur more often than they should (e.g., Leon, Ghidaoui, Schmidt, & García, 2009; Leon, Ghidaoui, Schmidt, & García, 2010). These overflows contain not only stormwater but also untreated human and industrial waste, toxic materials, and debris. They are a major water pollution concern for approximately 772 cities in the U.S. that have combined sewer systems (EPA, 2004).

Geysers have been studied over three decades in terms of water phase only or air-water interaction (e.g., Guo & Song, 1991; Vasconcelos, 2005; Lewis, 2011; Wright et al., 2011). A considerable number of hypothesis were formulated for the causes of geysers in stormwater and combined sewer systems. Guo and Song (1991) hypothesized that geysers are mainly caused by "the impact force of the rising water". These authors argued that if a dropshaft is well ventilated, the manhole cannot be blown off by air pressure alone. Later, Vasconcelos (2005) argued that the dropshaft hydrodynamics can be influenced by the presence of air pockets. More recently, Wright et al. (2011) discussed that the pressure from the sewer flow alone would not have been enough to raise the water level in the vertical shaft event to near the ground surface. Along the same reasoning of Wright et al. (2011); Lewis (2011) argued that with an "inertia-induced surge" alone, geysers cannot be explained entirely.

Even though geysers were studied for a relatively long time, their violent behaviour was neither reproduced experimentally nor numerically. In particular, it is not clear how to predict a large geyser height as observed in actual stormwater and combined sewer systems. For instance, for a geyser eruption to rise a height of 20 meters, the velocity of the gas-liquid mixture at the manhole exit would need to be about 20.4 m/s ($\sqrt{2gH}$, where H is the eruption height). It is cautioned that the ballistic equation ($w = \sqrt{2gH}$) is intended for a single-phase flow and not a spray-like (e.g., air-water mixture) flow as is the case for geysers, however it can still provide a rough estimate (e.g., Karlstrom et al., 2013). Also, it is not clear the reasons for consecutive eruptions, where the

first eruption is not the strongest in terms of height and velocity. For instance note in the YouTube video (`http://www.youtube.com/watch?v=4aQySL0sKys`) that for the first geyser (0:08-0:36) and the second geyser (1:26-1:42) the strongest eruption is definitely not the first one but the later ones. Hence, it can be inferred that the processes that lead to the occurrence of violent geysers are not yet well understood. The motivation of this article is to describe the mechanisms that lead to violent geysers in stormwater and combined sewer systems and to derive the upper limit for the geyser eruption velocity in these systems. This paper is divided as follows. First, based on laboratory observations, the mechanisms that lead to violent geysers in stormwater and combined sewer systems are described. Second, based on a mathematical analysis, the upper limit for the geyser eruption velocity is derived. Third, the derived upper limit for the geyser eruption velocity is assessed using two test cases: A geyser event in a stormwater collection system in Minneapolis and our laboratory experiments. Finally, the key results are summarized in the conclusion.

2 Mechanisms that lead to geysering in stormwater and combined sewer systems

The mechanisms described below are supported with laboratory observations of the author, whose research group has produced violent eruptions in a laboratory setting for the first time. The experiments took place at Oregon State University in Corvallis during June and July of 2016. For an in-depth description of the experimental setup and results, the reader is referred to Leon, Elayeb, and Tang (2018). Two types of experiments were performed, namely non-visualization and visualization. The non-visualization experiments focused on finding geyser heights for an array of conditions, which results can be found in Leon et al. (2018). The visualization experiments were intended to video filming the processes leading to violent geysers, the results of which are used in this paper. To facilitate the measurement of the geyser height, the present experiments were focused on a vertical pipe completely full of water, which may not represent field conditions. The role of smaller initial water depths on geyser intensity will be investigated in a subsequent study.

The apparatus for our experimental study consisted of a horizontal and vertical pipe, both of which were clear PVC with an internal diameter of 152.4 mm ($6''$). The upstream tank, which was located 6.3 m upstream of the vertical pipe, has a total volume of 1.7 m^3 (450 U.S. gallons). The upstream tank is connected to the horizontal pipe through a 152.4 mm gate valve, which controls the flow from the head tank. Another valve with 76.2 mm ($3''$) diameter was installed at the downstream end of the horizontal pipe to drain the water from the system. This downstream valve was closed during the experiments, which means that the initial velocity in the system was zero. Nine pressure transducers were used in the visualization experiments. The location of pressure transducers 2 to 8 are presented in Fig. 1. Pressure transducer 1 was located at the top of the upstream tank (see complete experimental setup in Leon et al., 2018).

The visualization experiments, which results are used in this paper, were limited to a vertical pipe length of 6m, an initial water volume in the tank of 0.9615 m^3 and an initial absolute air pressure head in the tank of 30.9 m. This pressure head is only used to drain the water out of the tank in such a way that when the upstream valve is fully opened the water level in the tank is at its bottom (i.e., air has occupied the entire tank) and at this point the system is in apparent equilibrium and the pressure head in the tank and anywhere in the horizontal pipe is 6 m (e.g., see pressure heads before 113.5 seconds in Fig. 2). If after opening the valve, the water level in the tank was significantly above its bottom (e.g., more than about 10 mm), geysering did not occur as the air in the tank was never admitted into the horizontal pipe. The latter means that before air entered the horizontal pipe to produce geysering, the pressure gradient in the horizontal pipe was zero. The experimental procedure was as follows:

(1) Keeping the upstream gate valve fully closed, the upstream tank is partially filled with water
(2) The upstream tank is pressurized with air to a pre-specified pressure and the data acquisition

system (DAQ) started to acquire data.

(3) The upstream gate is fully opened. Once the gate is fully opened, the water level in the tank is at its bottom and the system is in apparent equilibrium. Shortly after this apparent equilibrium, the air-water interface at the bottom of the air tank oscillates up and down slightly which quickly grows and then leads to the air admission from the air tank to the horizontal pipe. The geyser eruptions would occur shortly after the air admission to the horizontal pipe. The propagation of the air pocket and the geyser processes are described later in this section.

(4) After the eruptions, the system is depressurized and the data recording is stopped. It is worth mentioning that in all geyser experiments, all air in the tank evacuated the system and the final water depth at rest in the horizontal pipe was between 10% to 50% of the pipe diameter.

Each geyser produced in the experiments consisted of several violent eruptions (three to eight) which lasted a few seconds with heights exceeding 30 meters measured from the top of the vertical pipe. It is worth mentioning that as shown in Leon et al. (2018), the scale effects for the geyser lab experiments are negligible. The violent eruptions produced resemble the characteristics of those that occurred in actual stormwater and combined sewer systems. The laboratory observations are summarized in data of pressure transducers (Figs. 2-4), schematics (Figs. 5a-5f), video snapshots for vertical pipe (Fig. 6), and video snapshots for horizontal pipe (Fig. 7). The main mechanisms that lead to geysering can be summarized as follows:

(1) A large air pocket, which is formed during the filling of near-horizontal tunnels (e.g., Vasconcelos, 2005), approaches the dropshaft. This can be observed in Figs. 5a and 7.1.

(2) The large air pocket enters the dropshaft and rises due to buoyancy. The front of the air pocket, which resembles the classical Taylor bubble, occupies almost the entire cross-sectional area of the dropshaft. The tail of the air pocket ascending in the dropshaft is highly turbulent with a near homogenous mixture of air and water with great content of void fraction. In a similar way to the classical Taylor bubble, as the air pocket ascends, a significant amount of liquid that is on top of the air pocket is carried upwards and a portion of the water falls on the sides of the pocket (e.g., film flow). This can be observed in Figs. 5b and 6.1.

(3) When the Taylor-like bubble reaches the top of the dropshaft, most of the water that is on top of the air pocket is spilled (Fig. 5c).

(4) As water is quickly lost due to spilling, the hydrostatic pressure in the dropshaft is rapidly reduced, which accelerates the air entering the dropshaft. The rapid acceleration of air leads to a weak eruption from the dropshaft (Fig. 5d). Subsequently, the rapid increase in air velocity in the horizontal pipe results in the Kelvin-Helmholtz (KH) instability that transforms the initial stratified flow regime (Fig. 7.2) to wavy and, eventually, slug flow, which is a series of liquid plugs (slugs) separated by relatively large air pockets. The liquid slugs have some entrained air. The aforementioned wavy air interfaces and slugs can be observed in snapshots 3 to 35 in Fig. 7. During this process, the flow in the dropshaft is highly mixed and turbulent (see Fig. 6.2).

To verify the hypothesis that the transition from the initial stratified flow regime to slug flow is due to Kelvin-Helmholtz (KH) instability of the waves, we can use the following empirical fitted KH instability criteria (e.g., Kordyban, 1990):

$$U_G - U_L > 0.5\sqrt{(\rho_L - \rho_G) g h_G / \rho_G} \tag{1}$$

where U_G is the gas (i.e., air) velocity, U_L is the liquid (i.e., water) velocity, ρ_L is the density of liquid, ρ_G is the density of gas, g is acceleration of gravity and h_g is the depth of gas at equilibrium level. For air and water at 20 °C, $\rho_L = 1000$ kg/m^3, $\rho_G = 1.2$ kg/m^3. From the first two snapshots in the horizontal pipe (Figs. 7.1 and 7.2), h_G is approximately 13 mm.

Also, $U_L = 0$ because the downstream gate in the horizontal pipe is closed. Substituting values into Eq. (1), the KH instability criteria gives $U_G > 5.1$ m/s. Even though, the air velocity was not explicitly measured in the experiments, by comparing flow features in different frames (snapshots) in Fig. 7, the velocity of the air could be estimated. These velocities can easily exceed 5 m/s implying that the transition from the initial stratified flow regime to slug flow may be due to Kelvin-Helmholtz (KH) instability. It is worth mentioning that the KH instability provide a mechanism for initiating jumps and transitions, however after one or few slugs are weakly formed, the dynamics of the slugs (e.g., violent propelling) including their growth are governed by the pressure gradients between the slugs and the dropshaft.

(5) Once the slugs are formed in the horizontal pipe, they are violently propelled into the dropshaft right after a sudden drop of pressure in the dropshaft (e.g., after the previous eruption). During this process, new slugs can be formed in the horizontal pipe. The slugs in the horizontal pipe are propelled in bursts, each of which may result in a new eruption. The propelling of liquid slugs is activated whenever a significant pressure gradient between the horizontal pipe and the dropshaft is attained. Note in Figs. 2-4 that geyser eruptions (e.g., large pressure fluctuations at transducer 9), are preceded by large pressure gradients between the horizontal pipe (e.g., transducers 4 and 6) and the dropshaft (e.g., transducer 8). Note also in Figs. 2-4 that the pressures located downstream of the vertical pipe (transducers 6 and 7) have significant fluctuations around the mean pressure. According to the so-called Joukowsky equation, a pressure surge occurs when a fluid in motion is forced to stop or change velocity suddenly. In the geyser experiments, the flow velocity at the downstream end of the pipe is zero (e.g., dead end). However, the flow velocity in the horizontal pipe, upstream of the vertical pipe, may be very high as a result of the eruptions in the vertical pipe. Thus, there is a significant change of velocity in the downstream horizontal pipe (from large velocity at the vertical pipe to zero at the downstream end), which would lead a significant pressure surge. Note in Figs. 2-4 that the pressure trace at transducer 8 follows a similar pressure oscillation pattern to that of transducer 6, although with a slight delay. This means that pressure transients in the horizontal pipe are propagated to the dropshaft, and hence, pressure transients can also have an impact on geyser eruptions as they may lead to larger pressure gradients. Note also in Fig. 4 that the pressure head at transducer 2 decays slowly and it is not significantly affected by the pressure head oscillations at transducer 8. This is because of the discontinuity produced by the slugs, which block the uniform release of air from the horizontal pipe. The slow decay of pressure head in the horizontal pipe, due to the slugs, provides the pressure to still achieve significant pressure gradients (between the horizontal pipe and dropshaft) after the first geyser eruption. It is worth mentioning that the liquid slugs supply the water for the eruptions. Overall, the second or third geyser eruption has the largest intensity in terms of height (Fig. 5e).

(6) After the second or third eruption, there may be a few more eruptions, however as water is lost at the top of the dropshaft and the horizontal pipe around the dropshaft is depressurized, the geysering is terminated. On average we observed between 3 to 8 eruptions in a time frame of 2 to 10 seconds. After the eruptions are terminated, the water depth at rest in the horizontal pipe is between 10% to 50% of the pipe diameter (see Figs. 5f and 7.36). The violent propelling of slugs was reported in various studies of two-phase flows (e.g., Wallis & Dodson, 1973; Grotjahn & Mewes, 2007).

3 Upper limit for the geyser eruption velocity in vertical shafts

The aim of this section is to derive the upper limit for the geyser eruption velocity in vertical shafts. The assumptions of this derivation are listed below:

- The air-liquid mixture is assumed to be homogeneus (well mixed) during the geysering.
- The liquid is assumed to have a constant density (e.g., independent of pressure).
- The air gas is ideal and it is assumed to follow the isothermal process.

The compressible Navier-Stokes equations for the vertical direction (z) assuming a one-dimensional flow can be written as (Shapiro, 1954; Leon, 2016):

$$\frac{\partial \rho}{\partial t} + \frac{\partial (\rho w)}{\partial z} = 0 \tag{2}$$

$$\frac{\partial w}{\partial t} + \frac{1}{\rho}\frac{\partial p}{\partial z} + w\frac{\partial w}{\partial z} = -g - \frac{f}{2D}w^2 \tag{3}$$

where t is time, p is pressure, ρ is the density of the gas-liquid mixture, g is the gravitational acceleration, z is vertical distance measured from the dropshaft bottom, w is the velocity and f is the Darcy-Weisbach friction factor. Noting that the sound speed in the flow (a) is given by $\sqrt{dp/d\rho}$, Eq. (2) can be rewritten as:

$$a^2\frac{\partial w}{\partial z} + \frac{1}{\rho}\left(\frac{\partial p}{\partial t} + w\frac{\partial p}{\partial z}\right) = 0 \tag{4}$$

Combining Eqs. (3) and (4), the following equation is obtained:

$$\frac{1}{\rho}\frac{\partial p}{\partial z}\left(\frac{w^2}{a^2} - 1\right) = g + \frac{f}{2D}w^2 + \frac{\partial w}{\partial t} - \frac{w}{\rho a^2}\frac{\partial p}{\partial t} \tag{5}$$

Note in the right side of Eq. (5) that the first (gravity) and second (friction) terms are positive. Note also that for an accelerating flow in the vertical direction, $\partial w/\partial t$ is positive. With the sole purpose of finding the sign of $\partial p/\partial t$ in Eq. (5) let's make use of a Bernoulli-like equation, which applies to an unsteady frictionless and compressible flow in a stream tube and is given by (Fox, McDonald, Pritchard, & Mitchell, 2015; MIT, 2017)

$$wdw + \frac{\partial w}{\partial t}dz = -\frac{1}{\rho}dp - gdz \tag{6}$$

Even though the Momentum equation (Eq. 3) includes a friction term, the use of the Bernoulli-like equation(Eq. 6), which strictly applies to frictionless flow, is justified because these two equations (Eqs. 3 and 6) are not combined into a single equation. Instead, the Bernoulli-like equation(Eq. 6) is used for establishing qualitatively how the pressure changes with a change in velocity. By expanding the differentials dw and dp in Eq. (6) as partial derivatives with respect to the variables t and z and by setting $dz \to 0$, Eq. (6) can be simplified as follows:

$$w\frac{\partial w}{\partial t}dt = -\frac{1}{\rho}\frac{\partial p}{\partial t}dt \tag{7}$$

Note in Eq. (7) that for an accelerating flow in the vertical direction, $\partial w/\partial t$ is positive and thus, $\partial p/\partial t$ needs to be negative. Hence, all terms in the right side of Eq. (5) are positive. In addition, note that $\partial p/\partial z$ in the left side of Eq. (5) is negative. Thus, for Eq. (5) to be valid, the following

condition needs to be satisfied:

$$w < a \tag{8}$$

Note in Eq. (5) that even though the upper limit of the geyser eruption velocity is the gas-liquid mixture sound speed, w can never reach the value of a as to maintain the positive terms on the right hand side of Eq. (5). Note also in Eq. (5) that as w increases, the magnitude of the term $w^2/a^2 - 1$ decreases and thus, the magnitude of $\partial p/\partial z$ needs to increase to maintain the positive terms on the right hand side of Eq. (5). The latter is expected as a larger pressure gradient would result in a larger geyser eruption velocity. Even though the geyser eruption velocity can never match the air-liquid mixture sound speed, the geyser eruption velocity can get close to the aforementioned sound speed as discussed in Section 4. This is an important finding as the air-liquid mixture sound speed can be easily calculated, which could be used to calculate impact force and other parameters that would be useful in the design of manholes for mitigating the adverse effects of geysers. The finding that the geyser eruption velocity can get close to the air-liquid mixture sound speed is actually not a surprising result as explained below. As mentioned earlier, the measured geyser heights in the experiments exceeded 30 m, which would result in a geyser eruption velocity of about 24.2 m/s using the ballistic equation. Even though the ballistic equation is not strictly applicable to air-liquid mixtures, it can give a rough estimate of the eruption velocity (Karlstrom et al., 2013). In the other hand, the sound speed in an air-water mixture can achieve very low values (as low as 20 m/s) for small pressures (e.g., 1 bar) and void fractions between 15% and 85% (see for instance Kieffer, 1977, pages 2898 and 2899). An equation for estimating the sound speed of a two-phase mixture is given by (Mastin, 1995):

$$a = \sqrt{\frac{k_l k_g}{\rho[(1-\phi)k_g + \phi k_l]}} \tag{9}$$

where ϕ is the volume fraction of gas (i.e., ratio of gas volume to total volume), k_l and k_g are the bulk modulus of liquid and gas, respectively. The author is not aware of any measurement of gas/water volume ratios during geysering in stormwater or combined sewer systems. However, the literature reports these measurements during geysering in the degassing of lakes Nyos and Monoun. Even though the processes of geysering in a stormwater system and those in degassing of lakes are clearly different, regardless of the processes, a geyser eruption involves a significant ratio of gas/water volume. In this paper, due to the lack of data of gas/water volume ratios during geysering in stormwater or combined sewer systems, the data for geysering in degassing of lakes Nyos and Monoun will be used. The measured gas/water volume ratios for geysering in the degassing of lakes Nyos and Monoun ranged from 2.9 to 9 (Halbwachs, Sabroux, Grangeon, Kayser, & Tochon-Danguy, 2004). The latter indicates that at eruption the values of ϕ would range between 0.74 and 0.90. As shown in Leon (2016), at eruption, Eq. (9) can be reduced to the equation below with good accuracy:

$$a \approx \sqrt{\frac{p_{atm}}{\phi(1-\phi)\rho_l}} \tag{10}$$

where p_{atm} is the absolute atmospheric pressure and ρ_l is the water density.

It is worth mentioning that in our laboratory experiments (Leon et al., 2018), the void fraction was not measured and hence, the "experimental" value of a cannot be directly compared with the maximum geyser eruption velocity.

4 The air-water mixture sound speed as a predictor for the maximum geyser eruption velocity

In this section we will discuss if the air-water mixture sound speed (Eq. 10) can be regarded as the upper limit for the maximum geyser eruption velocity. For this discussion, two test cases are considered: A geyser event in a stormwater collection system in Minneapolis and our laboratory experiments. For estimating the air-water mixture sound speed, data of gas/water volume ratios during geysering are necessary, which were not available for both test cases. The author is not aware of any measurement of gas/water volume ratios during geysering in stormwater or combined sewer systems. However, measurements of gas/water volume ratios are available for geysering in the degassing of lakes Nyos and Monoun. As mentioned earlier, even though the processes of geysering in a stormwater system and those in degassing of lakes are clearly different, regardless of the processes, a geyser eruption involves a significant ratio of gas/water volume. In this section, due to the lack of data of gas/water volume ratios during geysering in stormwater or combined sewer systems, the data for geysering in degassing of lakes Nyos and Monoun were used. The measured gas/water volume ratios in the degassing of lakes Nyos and Monoun ranged from 2.9 to 9 (Halbwachs et al., 2004), which give ϕ values between 0.74 and 0.90. The mixture density (ρ) is often approximated as $\rho \approx (1-\phi)\rho_l$ (e.g., Leon, 2016), which gives a mixture density ranging between 100 and 260 kg/m^3.

4.1 *Geyser event (July 11, 2004) in a stormwater collection system in Minneapolis*

This event occurred on July 11, 2004 at Interstate 35W (Minnesota), which data is available in Wright et al. (2011). According to Wright et al. (2011), the system is a 3.7-m high arch storm-water tunnel and the dropshaft is 2.4 m in diameter and 24.9 m in height. The reported eruption height was about 20 m (Wright et al., 2011), which results in a geyser eruption velocity of 19.8 m/s using the ballistic equation ($w \approx \sqrt{2gH}$). The barometric pressure for July of 2016 in Minnesota was about 29.9 in Hg (Usairnet, 2016), which is 101253 Pa.

Figure 8 shows the "observed" geyser eruption velocity together with the calculated sound speed in the air-water mixture for the range of mixture densities obtained from geyser measurements during the degassing of Lakes Nyos and Monoun. The results in Fig. 8 show that for the aforementioned range of mixture densities, the air-water mixture sound speed decreased about 32% for an increase of the density of the air-water mixture (e.g., as air volume reduces) of about 160%. The relatively slow reduction of the air-water mixture sound speed with an increase in the density of the air-water mixture implies that the air-water mixture sound speed can be well quantified even if the volume fraction of gas (i.e., ratio of gas volume to total volume) is not accurately estimated. The results in Fig. 8 also show that, as predicted by Eq. (8), the "measured" geyser eruption velocity does not exceed the air-water mixture sound speed for the entire range of mixture densities obtained during the degassing of Lakes Nyos and Monoun.

4.2 *Our laboratory work*

As shown in Leon et al. (2018), the geysers produced in our lab experiments resemble the characteristics of those that occurred in actual stormwater and combined sewer systems. The maximum geyser height measured from the top of the dropshaft was 32 meters, which results in a geyser eruption velocity of about 25 m/s using the ballistic equation. The barometric pressure for Corvallis, Oregon in June and July of 2016 was about 30.13 in Hg (Usairnet, 2016), which is 102032 Pa.

Figure 9 shows the maximum "observed" geyser eruption velocity together with the calculated air-water mixture sound speed for the range of mixture densities obtained from geyser measurements during the degassing of Lakes Nyos and Monoun. In a similar way to the Minneapolis geyser

case, the results in Fig. 9 show that for the aforementioned range of mixture densities, the air-water mixture sound speed decreased about 32% for an increase of the density of the air-water mixture (e.g., as air volume reduces) of about 160%. The latter was expected as the only variation between the two test cases is the atmospheric pressure, which does not change significantly. The results in Fig. 9 also show that for most of the aforementioned range of mixture densities, the air-water mixture sound speed exceeds the "observed" geyser eruption velocity. However, for a small range of mixture densities, the "observed" geyser eruption velocity exceeds slightly (< 2 m/s) the air-water mixture sound speed. As mentioned earlier, the void fraction was not measured in our laboratory experiments, and hence the "experimental" value of a cannot be directly compared with the maximum geyser eruption velocity. Because for most of the range of mixture densities, the air-water mixture sound speed exceeds the "observed" geyser eruption velocity and for the small remaining range the difference is only small (< 2 m/s), the air-water mixture sound speed (Eq. 10) can be deemed as the upper limit for the maximum geyser eruption velocity.

5 Conclusion

This paper describes the mechanisms that lead to violent geysers in vertical shafts and derives the upper limit for the geyser eruption velocity. The key results are as follows:

(1) The described mechanisms that lead to violent geysers in vertical shafts were supported with laboratory observations of the author, whose research group has produced violent geysers in a laboratory setting for the first time. Each geyser produced consists of a few consecutive violent eruptions within a time frame of a few seconds with heights that may exceed 30 m, measured from the top of the dropshaft. These characteristics resemble those geysers that occurred in actual stormwater and combined sewer systems.
(2) The air-water mixture sound speed (Eq. 10) can be deemed as the upper limit for the maximum geyser eruption velocity.
(3) The air-water mixture sound speed decreases slowly with an increase in the density of the air-water mixture for the typical range of volume fraction of gas (i.e., ratio of gas volume to total volume) observed in the geysering due to degassing of lakes Nyos and Monoun.
(4) the pressure gradient $\partial p/\partial z$ needs to increase substantially for the geyser eruption velocity to approach the air-water mixture sound speed. This is expected as a larger pressure gradient would result in a larger geyser eruption velocity.

Overall, this paper shows that according to theory, the maximum geyser eruption velocity cannot match or exceed the air-water mixture sound speed. The test cases show that this is the case, however the geyser eruption velocity can get close to the aforementioned sound speed.

Acknowledgements

The authors are grateful to the JHR anonymous reviewers for their constructive comments, which helped to significantly improve the quality of the manuscript.

Disclosure

This manuscript has not been formally reviewed by EPA. The views expressed are solely those of the author. EPA does not endorse any products or commercial services mentioned.

Funding

This work was supported by the U.S. Environmental Protection Agency [grant R835187].

Notation

a = sound speed (m s^{-1})
f = Darcy-Weisbach friction factor (–)
g = gravity acceleration (ms^{-2})
h_g = depth of gas at equilibrium level (m)
k_l = bulk modulus of liquid (Pa)
k_g = bulk modulus of gas (Pa)
p = pressure (Pa)
p_{atm} = absolute atmospheric pressure (Pa)
t = time (s)
U_G = gas (i.e., air) velocity in horizontal pipe (m s^{-1})
U_L = liquid (i.e., water) velocity in horizontal pipe (m s^{-1})
w = geyser eruption velocity (m s^{-1})
z = vertical distance measured from the dropshaft bottom (m)
ϕ = volume fraction of gas (i.e., ratio of gas volume to total volume) (–)
ρ = density of gas-liquid mixture (kg m^{-3})
ρ_G = gas density (kg m^{-3})
ρ_L = liquid density (kg m^{-3})

References

EPA. (2004). *Impacts and Control of CSOs and SSOs* (Report to Congress No. EPA 833-R-04-001). Office of Water (4203), Washington, D.C. 20460: United States Environmental Protection Agency.

Fox, R. W., McDonald, A. T., Pritchard, P. J., & Mitchell, J. W. (2015). *Introduction to Fluid Mechanics, 9th Edition SI Version*. Wiley.

Grotjahn, K., & Mewes, D. (2007). Transient behaviour of two-phase slug flow in horizontal pipes. In *Transient phenomena in multiphase and multicomponent systems* (pp. 103–118). Wiley-VCH Verlag GmbH & Co. KGaA. Retrieved from `http://dx.doi.org/10.1002/9783527610785.ch7`

Guo, Q., & Song, C. S. S. (1991). Hydrodynamics under transient conditions. *J. Hydraul. Eng*, *117*(8), 1042-1055.

Halbwachs, M., Sabroux, J. C., Grangeon, J., Kayser, G., & Tochon-Danguy, J. C. (2004). Degassing the "killer lakes" Nyos and Monoun, Cameroon. *Eos*, *85*, 281.

Karlstrom, L., Hurwitz, S., Sohn, R., Vandemeulebrouck, J., Murphy, F., Rudolph, M. L., ... McCleskey, R. B. (2013). Eruptions at Lone Star Geyser, Yellowstone National Park, USA, part 1: energetics and eruption dynamics. *Journal of Geophysical Research B: Solid Earth*, *118*(8), 4048-4062.

Kieffer, S. W. (1977). Sound speed in liquid-gas mixtures: Water-air and water-steam. *Journal of Geophysical Research*, *82*(20), 2895–2904. Retrieved from `http://dx.doi.org/10.1029/JB082i020p02895`

Kordyban, E. (1990). Horizontal slug flow: A comparison of existing theories. *Journal of Fluids Engineering*, *112*(1), 74-83.

Leon, A. S. (2006). *Improved modeling of unsteady free surface, pressurized and mixed flows in storm-sewer systems* (Unpublished doctoral dissertation). Univ. of Illinois at Urbana-Champaign, Urbana, IL.

Leon, A. S. (2016). Mathematical models for quantifying eruption velocity in degassing pipes based on exsolution of a single gas and simultaneous exsolution of multiple gases. *J. volcanology and geothermal research*, *323*(1), 72-79.

Leon, A. S., Elayeb, I., & Tang, Y. (2018). An experimental study on violent geysers in vertical pipes. *Journal of Hydraulic Research (In print)*.

Leon, A. S., Ghidaoui, M. S., Schmidt, A. R., & García, M. H. (2006). Godunov-type solutions for transient flows in sewers. *Journal of Hydraulic Engineering*, *132*(8), 800–813.

Leon, A. S., Ghidaoui, M. S., Schmidt, A. R., & García, M. H. (2009). Application of Godunov-type schemes to transient mixed flows. *Journal of Hydraulic Research*, *47*(2), 147–156.

Leon, A. S., Ghidaoui, M. S., Schmidt, A. R., & García, M. H. (2010). A robust two-equation model for transient mixed flows. *Journal of Hydraulic Research*, *48*(1), 44-56.

Lewis, J. M. (2011). *A physical investigation of air/water interactions leading to geyser events in rapid filling pipelines* (Unpublished doctoral dissertation). University of Michigan.

Mastin, L. G. (1995). A numerical program for steady-state flow of hawaiian magma gas mixtures through vertical eruption conduits. *U. S. Geol. Surv. Open-File Rep.*, 95.

MIT. (2017). *Advanced Fluid Mechanics notes of MIT Department of Mechanical Engineering.* Retrieved 2017-12-16, from `https://ocw.mit.edu/courses/mechanical-engineering/2-25-advanced-fluid-mechanics-fall-2013/inviscid-flow-and-bernoulli/MIT2_25F13_Shapi4.05_Solu.pdf`

Shapiro, A. (1954). *The dynamics and thermodynamics of compressible fluid flow, volume ii.* New York: The Ronald Press Company.

Usairnet. (2016). *Minnesota barometric pressure map.* Retrieved 2015-7-24, from `http://www.usairnet.com/weather/maps/current/minnesota/barometric-pressure/`

Vasconcelos, J. G. (2005). *Dynamic approach to the description of flow regime transition in stormwater systems* (Unpublished doctoral dissertation). University of Michigan.

Wallis, G. B., & Dodson, J. E. (1973). The onset of slugging in horizontal stratified air-water flow. *International Journal of Multiphase Flow*, *1*(1), 173 - 193. Retrieved from `http://www.sciencedirect.com/science/article/pii/0301932273900104`

Wright, S., Lewis, J., & Vasconcelos, J. (2011). Geysering in rapidly filling storm-water tunnels. *J. Hydraul. Eng*, *137*(1), 112-115.

List of Figures

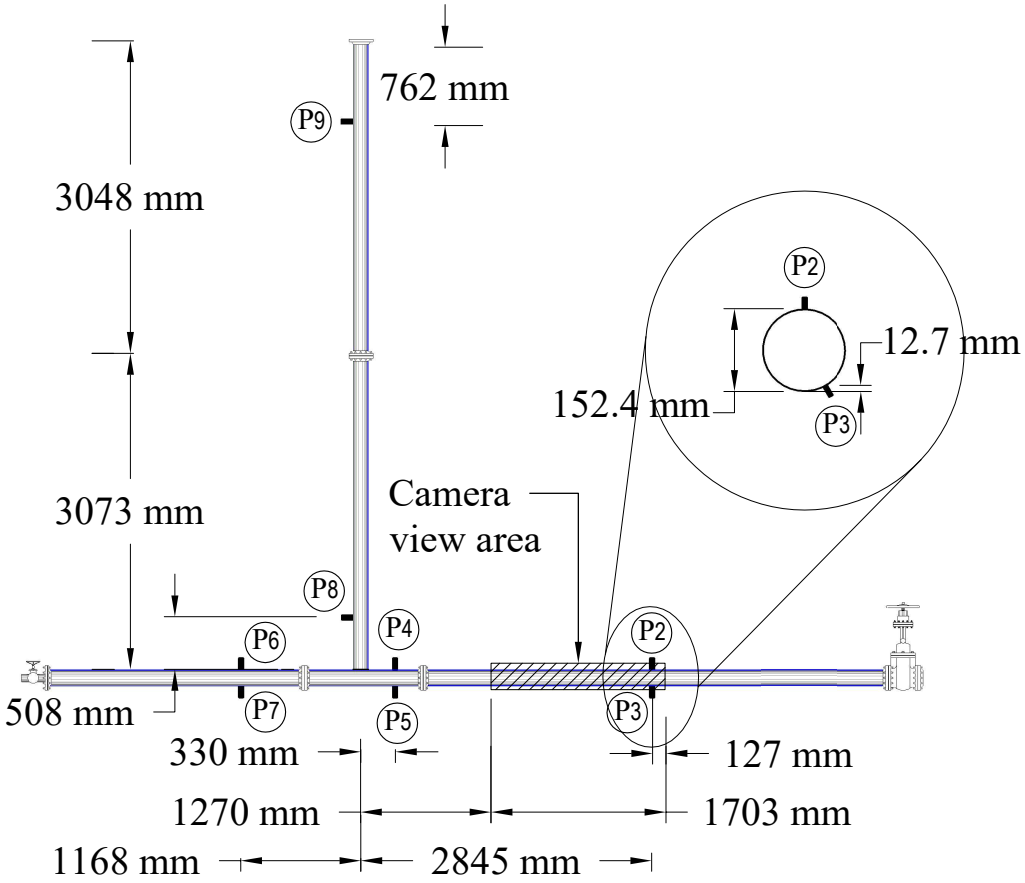

Figure 1: Location of pressure sensors for visualization experiments (Not To Scale)

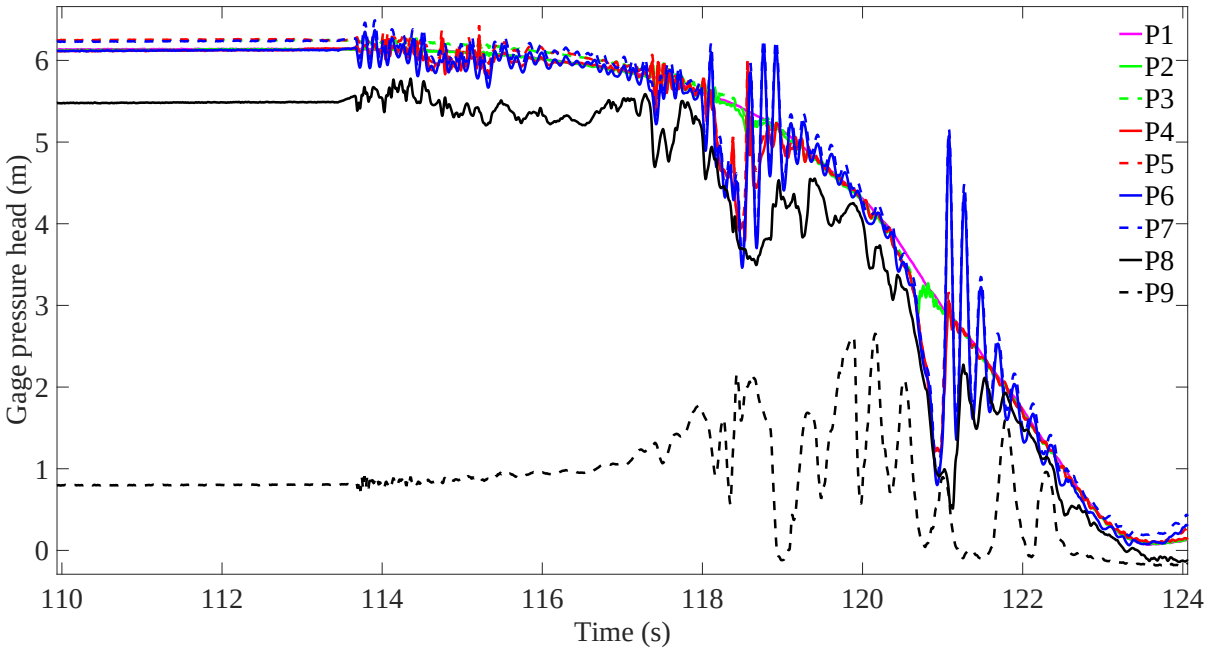

Figure 2: Example of pressure heads recorded in a geyser experiment (dropshaft height = 6 m)

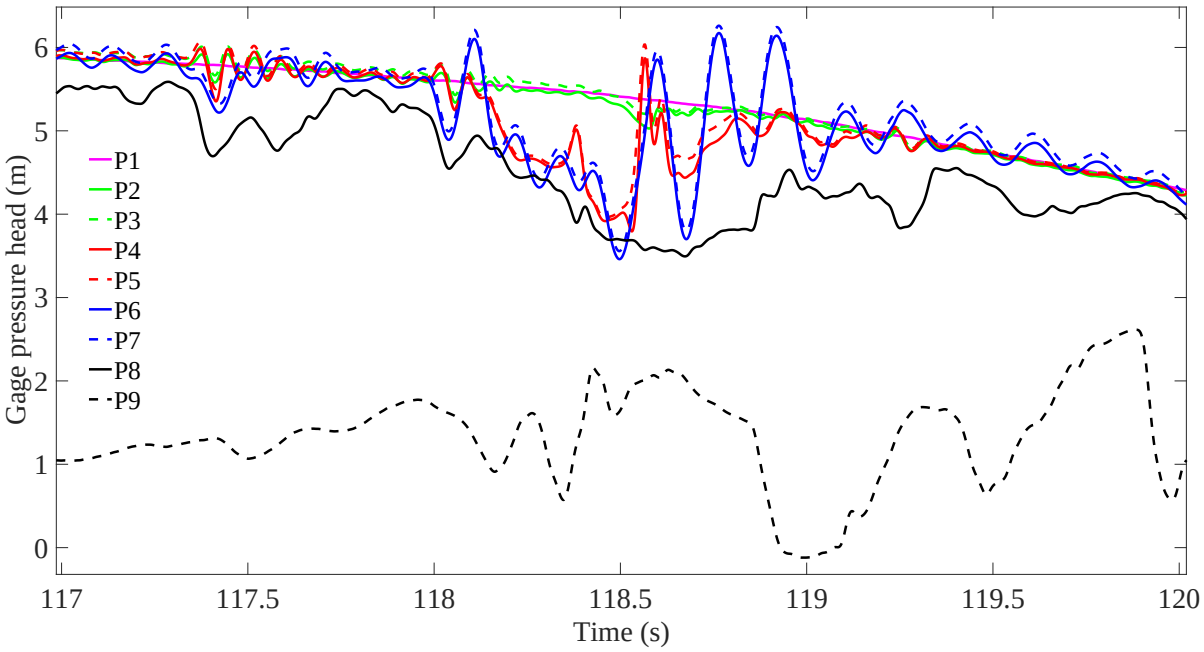

Figure 3: First zoom-in of Figure 2

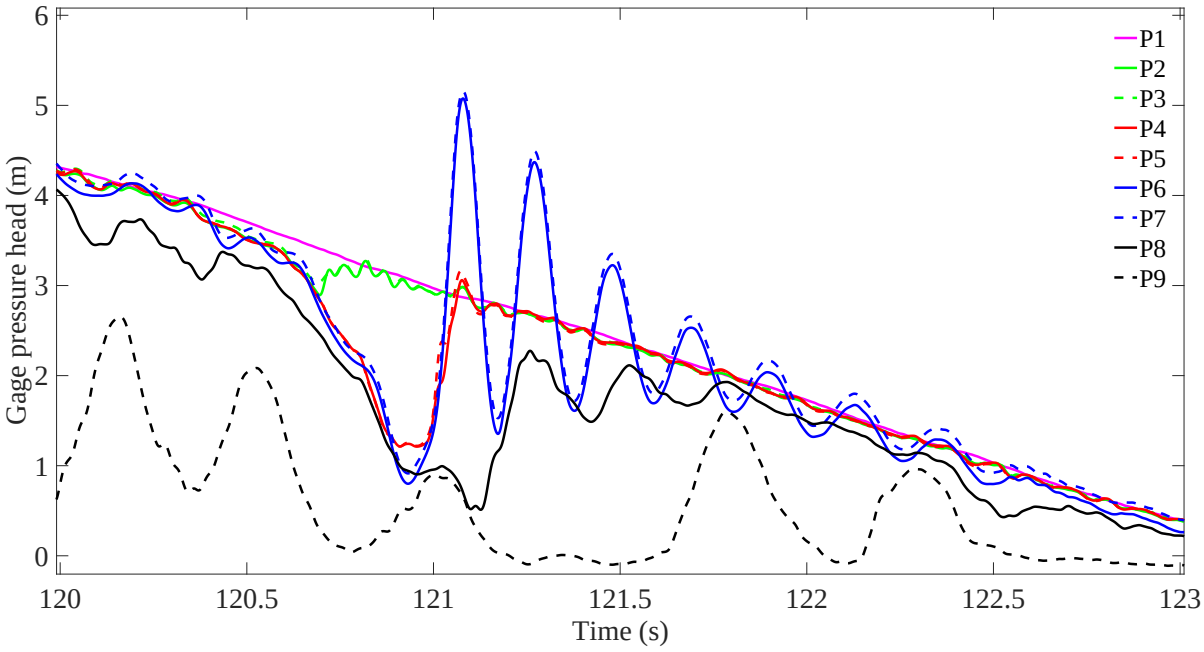

Figure 4: Second zoom-in of Figure 2

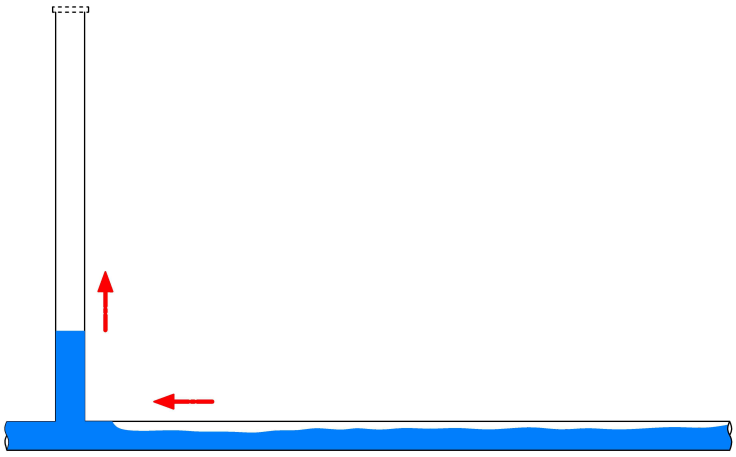

Figure 5: Geyser Processes (a) air pocket approaching dropshaft

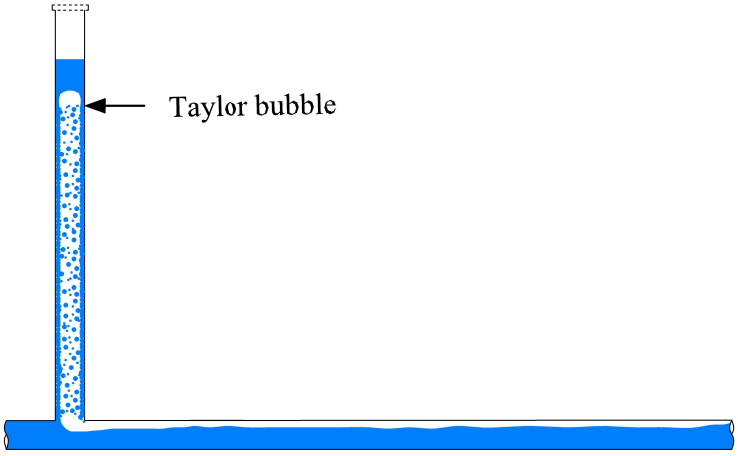

(b) Rising of Taylor-like bubble

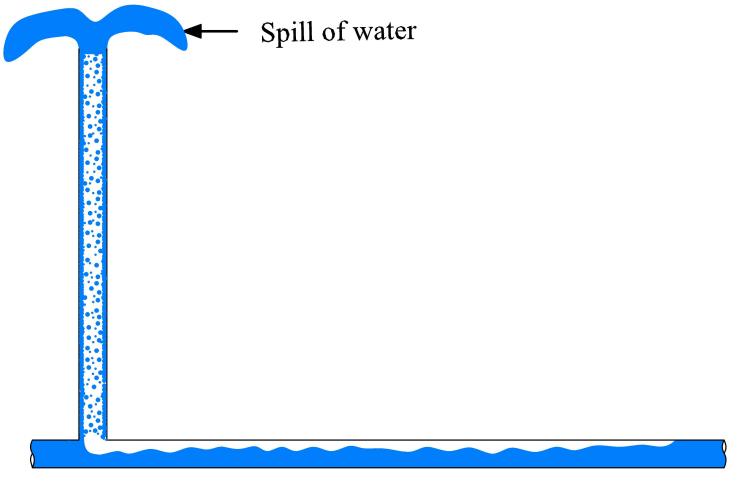

(c) Water spill and acceleration of air pocket in horizontal pipe

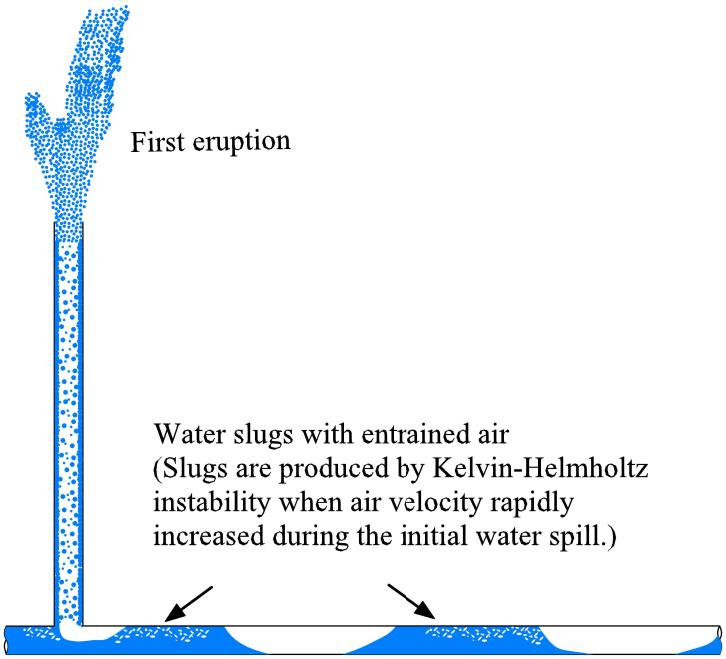

(d) First eruption and formation of liquid slugs

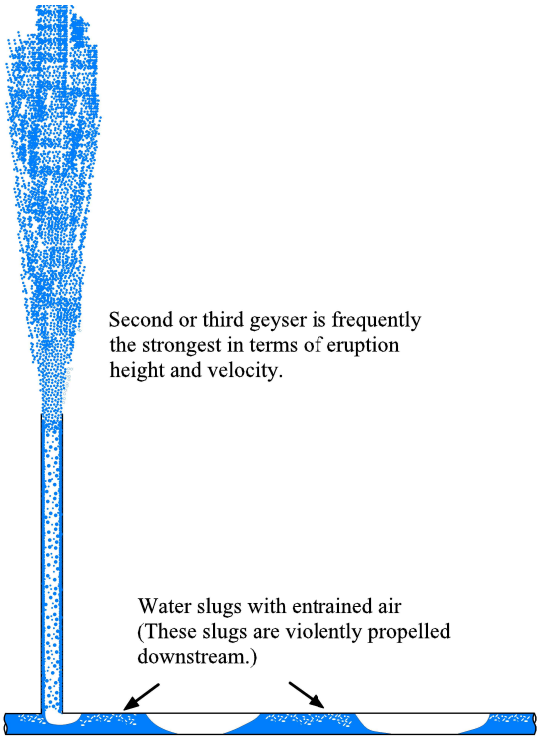

(e) Successive eruptions as a result of blowout of slugs

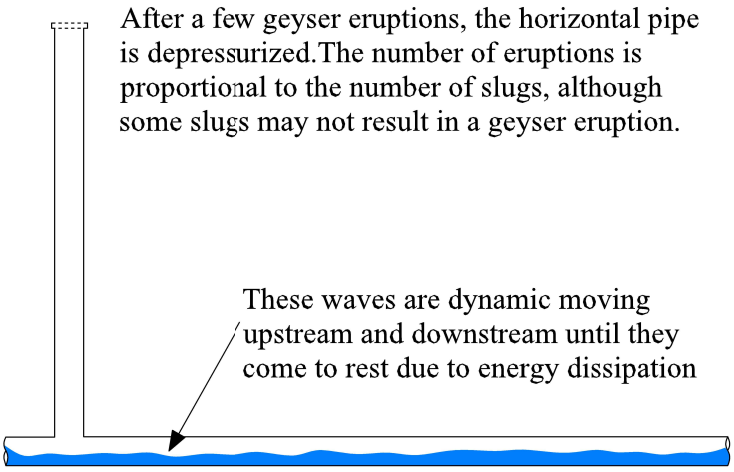

(f) Depressurization and propagation of waves in the horizontal pipe

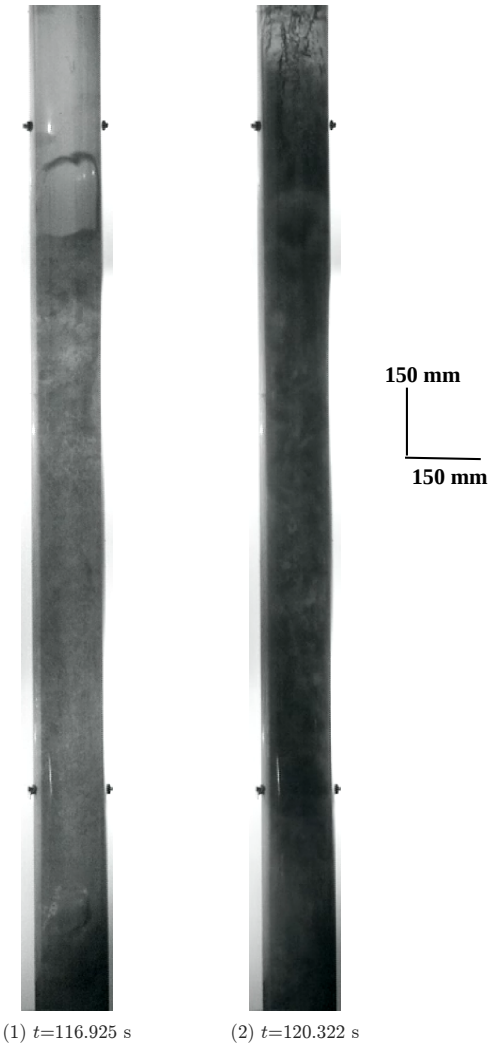

Figure 6: Flow snapshots in the experimental vertical pipe at various times

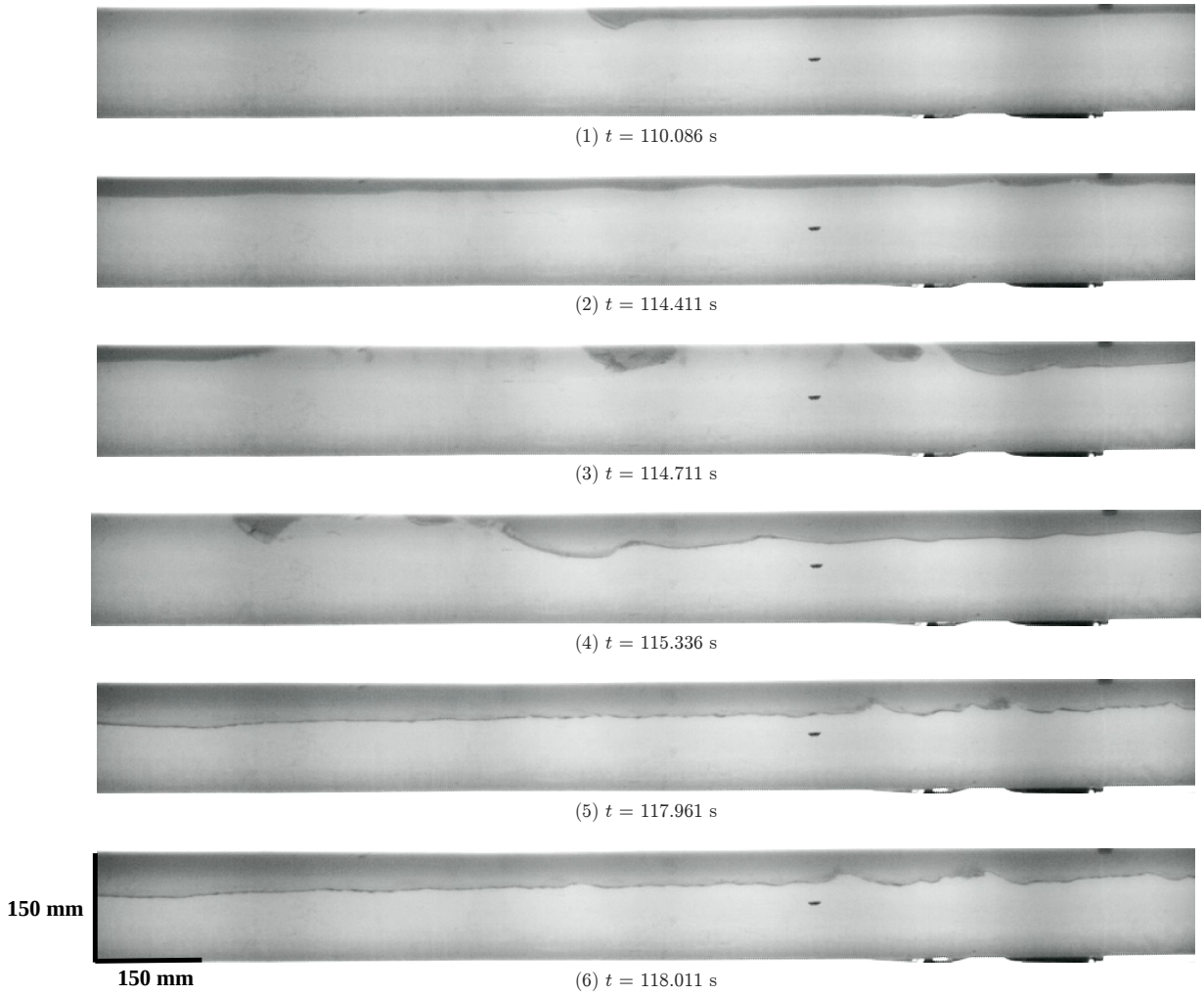

Figure 7: Flow snapshots in the experimental horizontal pipe at various times

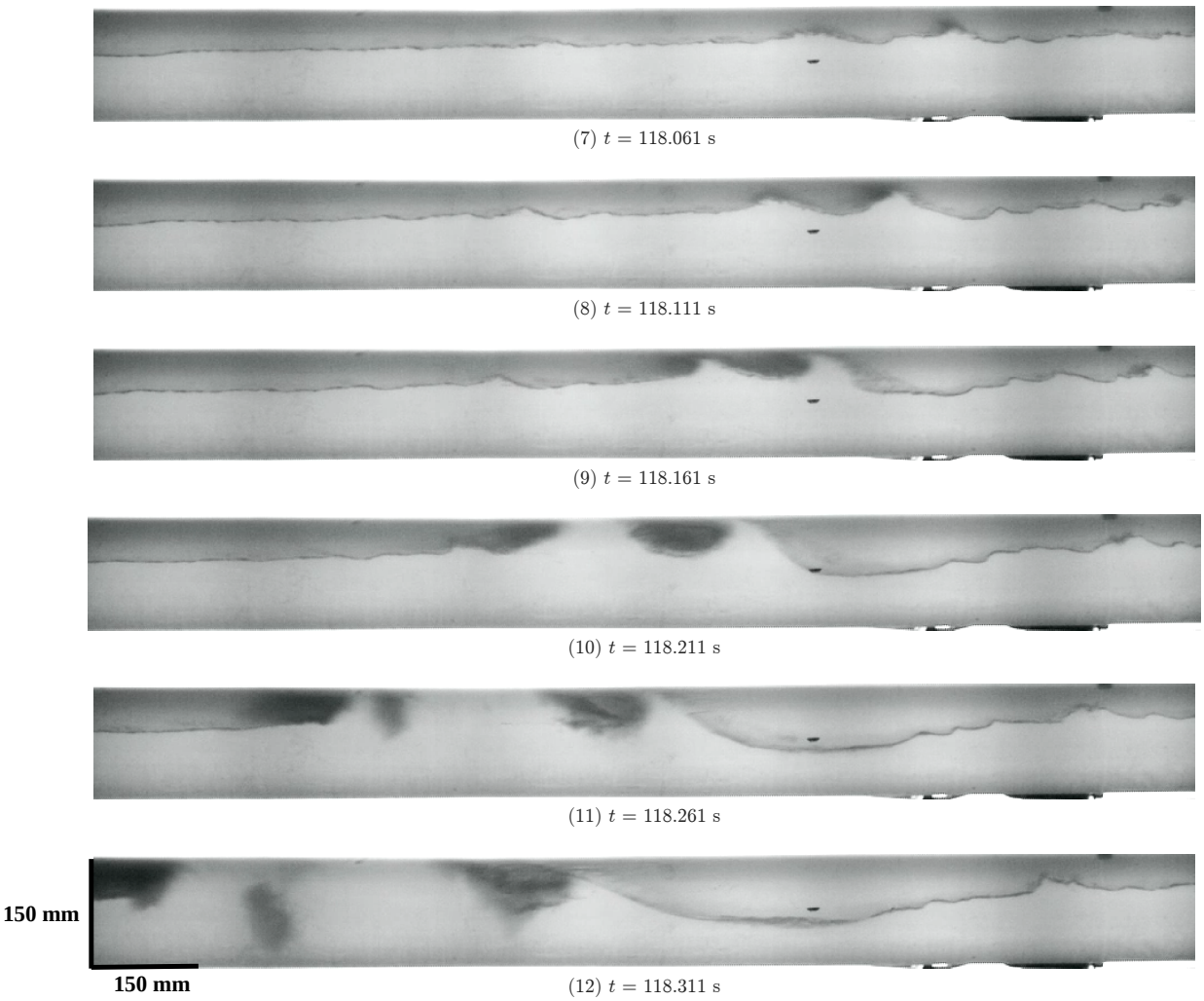

Flow snapshots in the experimental horizontal pipe at various times (Cont.)

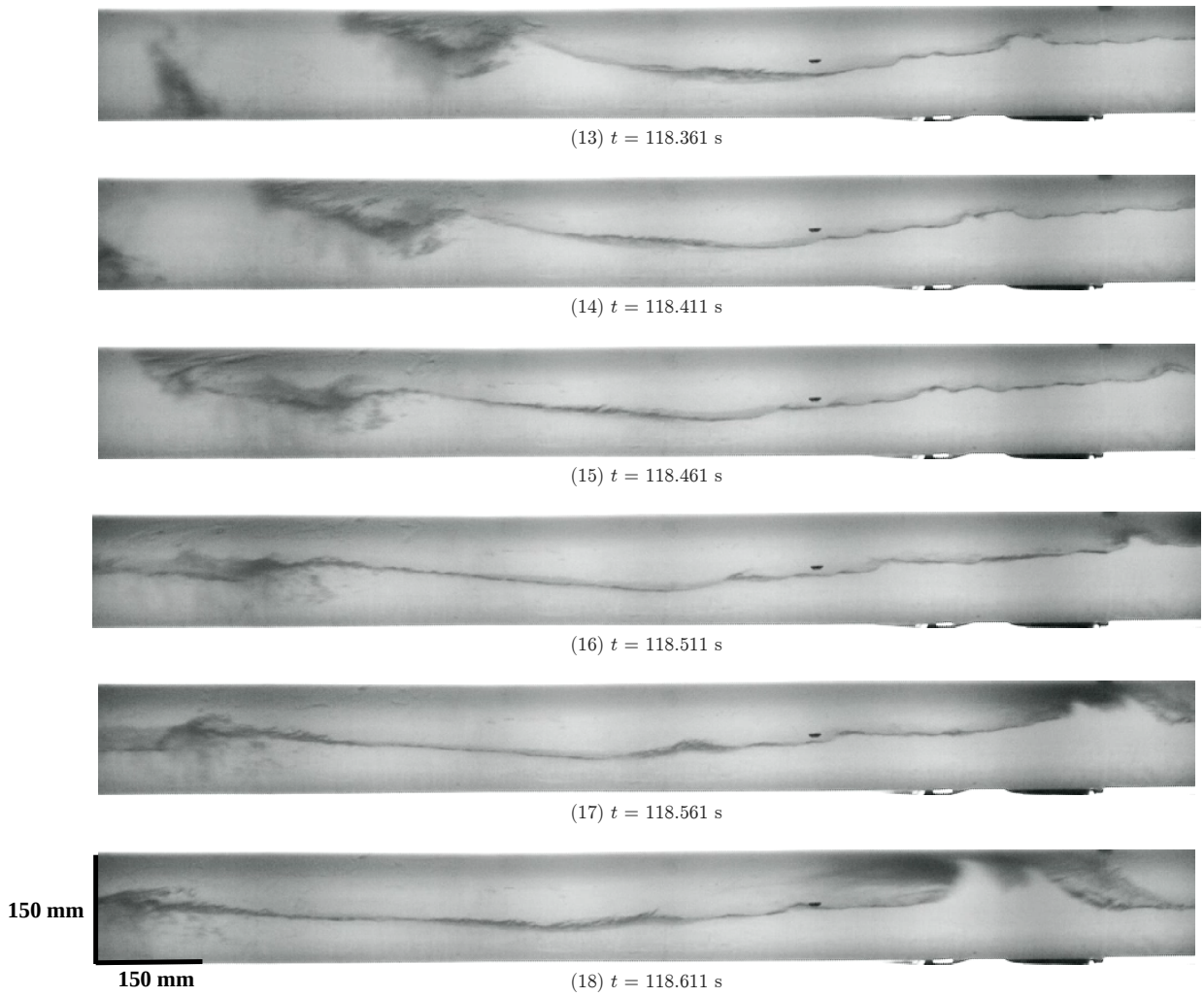

Flow snapshots in the experimental horizontal pipe at various times (Cont.)

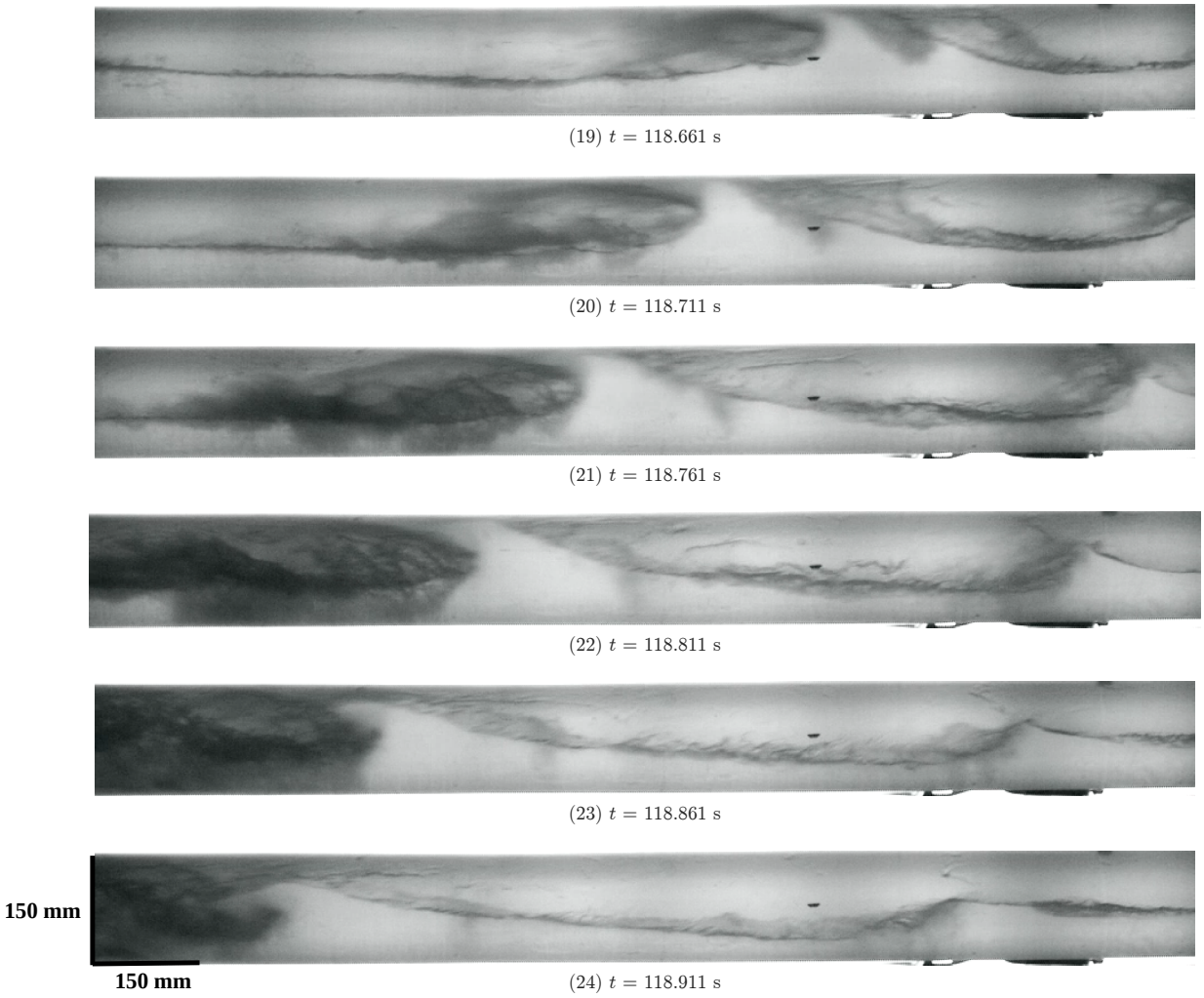

Flow snapshots in the experimental horizontal pipe at various times (Cont.)

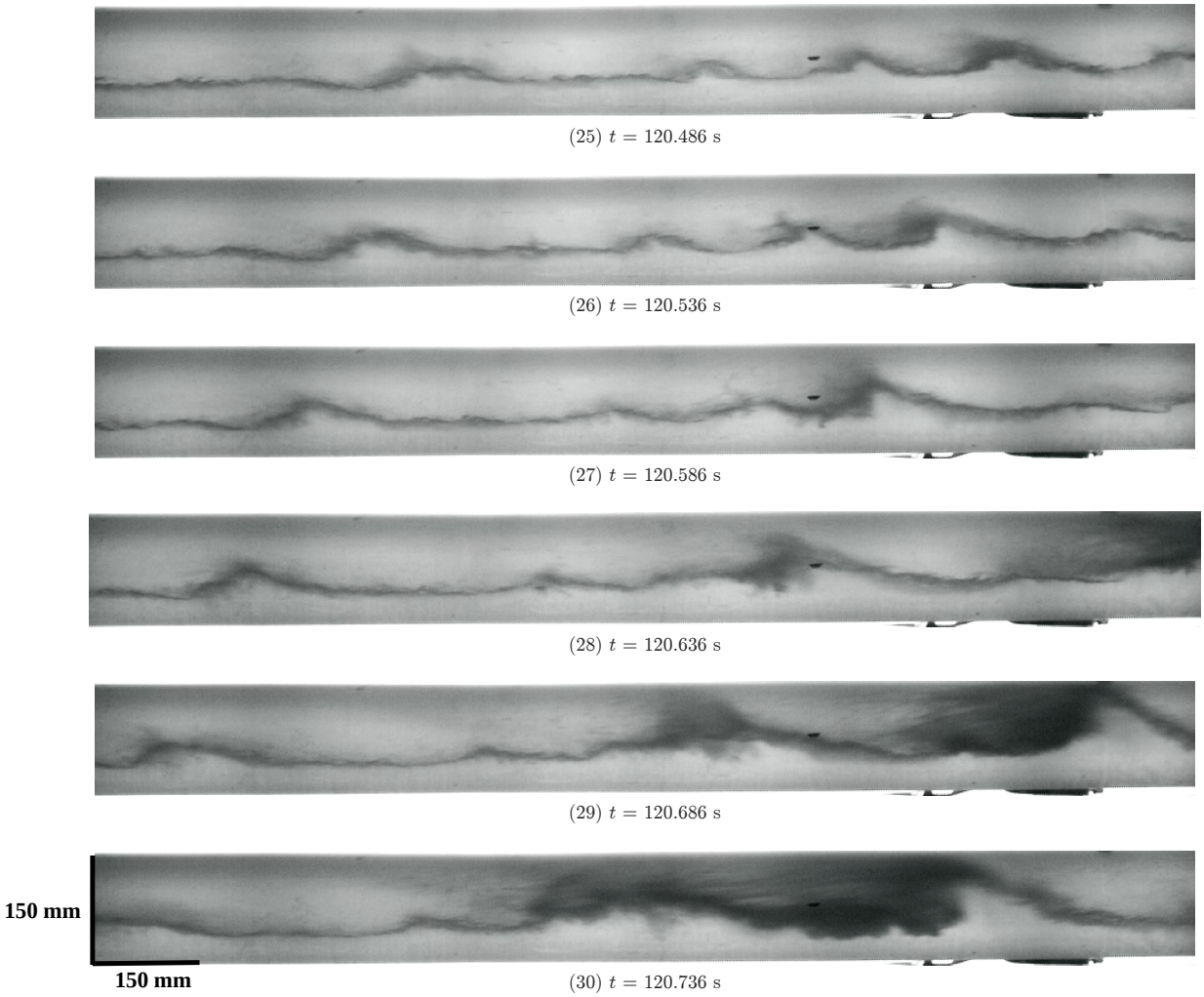

Flow snapshots in the experimental horizontal pipe at various times (Cont.)

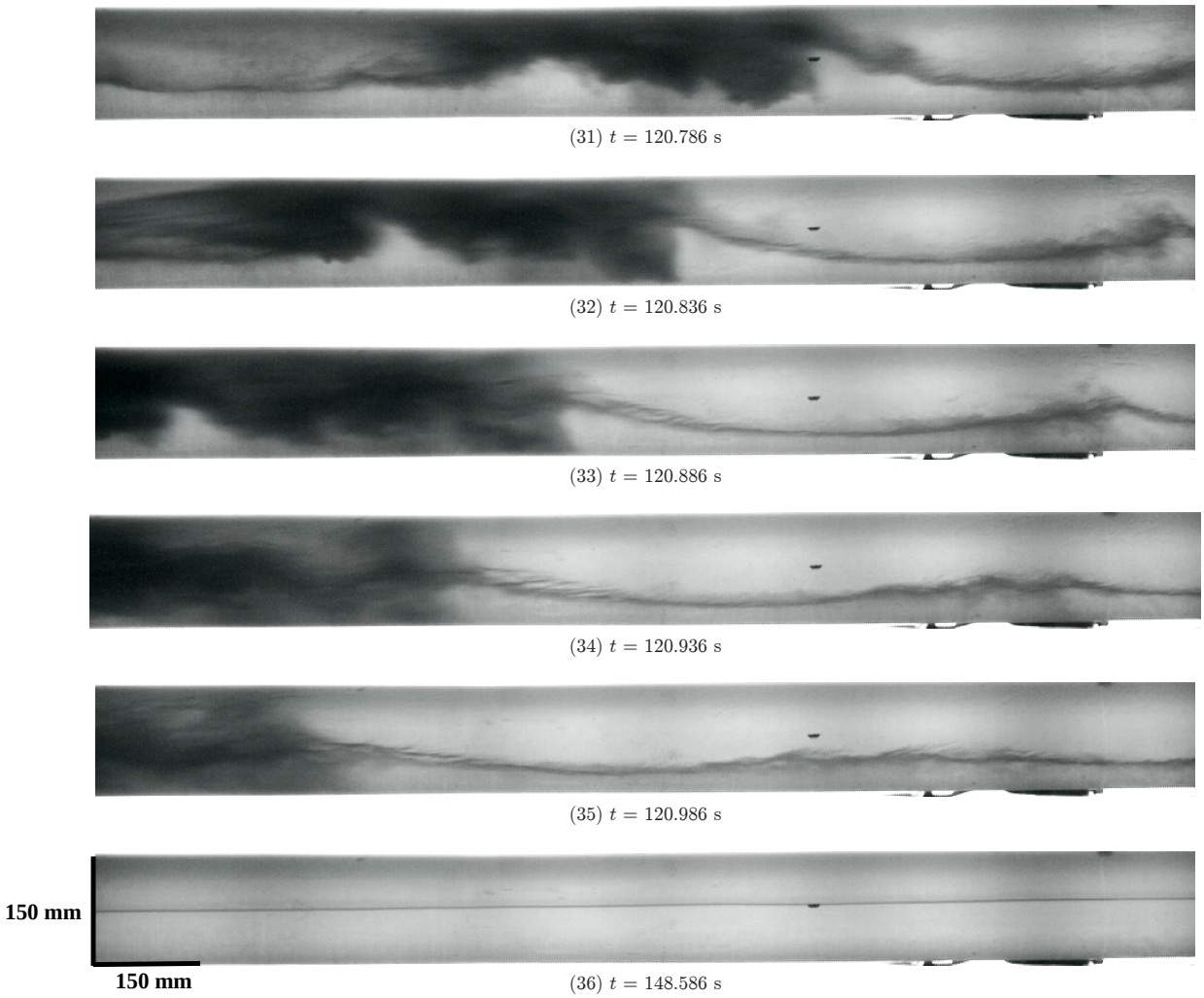

Flow snapshots in the experimental horizontal pipe at various times (Cont.)

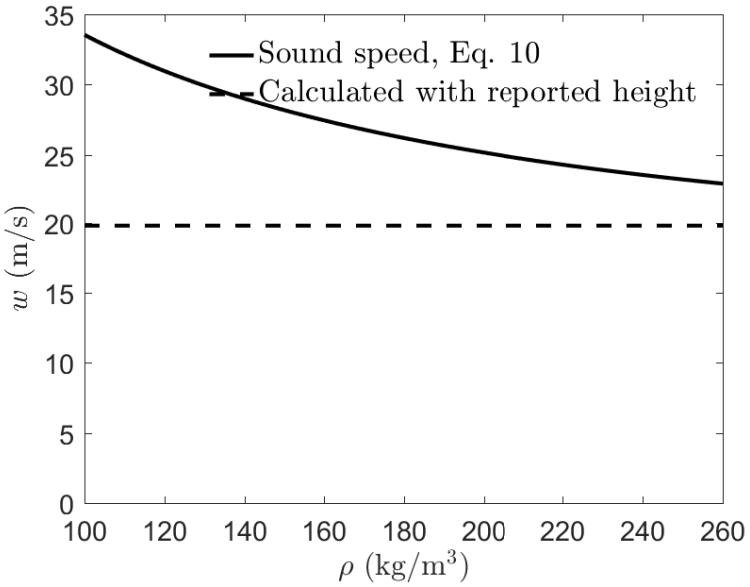

Figure 8: Air-water mixture sound speed as a predictor for the maximum geyser eruption velocity for the Minneapolis geyser on July 11, 2004

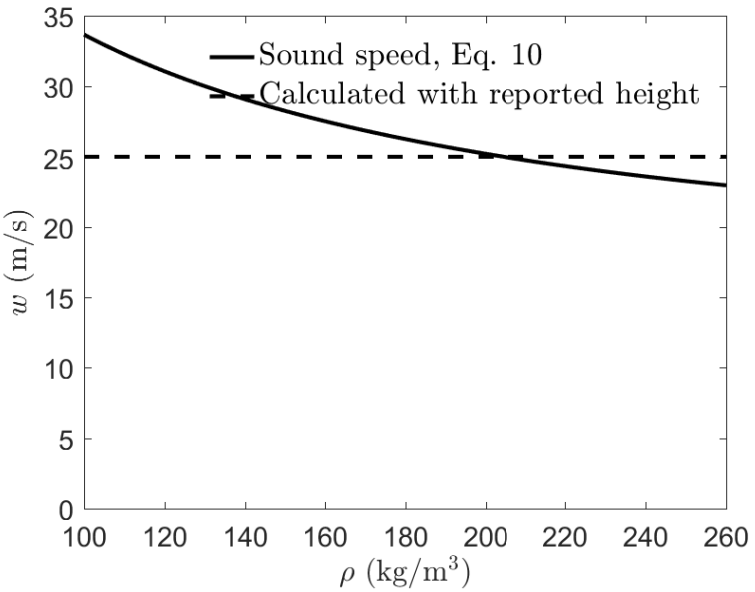

Figure 9: Air-water mixture sound speed as a predictor for the maximum geyser eruption velocity for our laboratory geysers